Formation of amorphous and icosahedral phases in Ti–Zr–Hf–LTM (LTM = Ni, Pd or Pt) alloys

N. Chen [a,*], D.V. Louzguine-Luzgin [b], T. Kubota [a], S. Ranganathan [c], A. Inoue [b]

[a] *Department of Materials Science, Graduate School, Tohoku University, Sendai 980-8577, Japan*
[b] *Institute for Materials Research, Tohoku University, Sendai 980-8577, Japan*
[c] *Department of Metallurgy, Indian Institute of Science, Bangalore 560012, India*

Abstract

A nanoscale icosahedral (I) phase was formed in the melt-spun $Ti_{40}Zr_{20}Hf_{20}(LTM)_{20}$ (LTM = Ni, Pd, or Pt) alloys. However, in Pd-bearing alloy it is presumed to be a distorted I-phase or a high-order approximation. I phase, Hf_2Pt and β-(Ti, Zr, Hf, Ni) solid solution phases are formed in the arc-melted $Ti_{40}Zr_{20}Hf_{20}Pt_{20}$ ingot.

Keywords: Quasicrystals; Rapid solidification; Microstructure

1. Introduction

Since the icosahedral (I) phase was discovered in a rapidly solidified Al–Mn alloy by Shechtman et al. [1], nanoscale I phase has been found in various alloy systems including Zr [2–4], Hf [5,6] and Cu [7,8] based alloys. Thermodynamically stable I alloys have also been formed in Ag–In–Ca, Cd–Ca, Cu–Ga–Mg–Sc and Ti–Zr–Ni systems, etc. [9–12]. Extensive studies on I phase formed in Ti–Zr–Ni system have been carried out because of its large capacity for hydrogen storage [13,14]. It was reported that $Ti_{40}Zr_{40}Ni_{20}$ is nearly the optimal quasicrystal forming composition, which lies at the crossing point of the two specific lines, termed as e/a-constant and e/a-variant lines [15]. As I phase can be formed in Zr–Pt, Zr–Pd [16–18] and Ti–Zr–Ni [12], it has been suggested and shown that Zr and Hf being part of the IVA group elements can be substituted in I phase of Ti–Zr–Hf–Ni alloy because of their chemical similarity [19].

In the present work we study the formation of the quasicrystalline phase in the $Ti_{40}Zr_{20}Hf_{20}LTM_{20}$ alloys (LTM indicates a late transition metal, Ni, Pd or Pt which belong to the same VIIIA group) containing Hf which partially (by 50%) substitutes Zr.

2. Experimental procedure

Ingots of $Ti_{40}Zr_{20}Hf_{20}(Ni, Pd, Pt)_{20}$ alloys were prepared by arc-melting the mixtures of pure Ti, Zr, Hf, Ni, Pd and Pt metals in a Ti-gettered argon atmosphere. The purity of the early transition metals was over 99.8 mass% while the late transition metals were of 99.9 mass% purity. From these alloy ingots, ribbon samples of 0.6–1.5 mm in width and 23–32 μm in thickness were prepared by rapid solidification of the melt on a single copper roller at a surface velocity of 40 m/s in an argon atmosphere. The structure of the samples was examined by X-ray diffractometry (XRD) with monochromatic

* Corresponding author. Tel.: +81 222 152 220; fax: +81 222 152 111.
E-mail address: asyzxy@imr.edu (N. Chen).

Cu K_α radiation. The phase transformations were studied by differential scanning calorimetry at a heating rate of 0.67 K/s. The microstructure was examined by transmission electron microscopy (TEM) using a JEM 2010 (JEOL) microscope operating at 200 kV. The samples for TEM were prepared by the ion polishing technique.

3. Results and discussion

The XRD patterns of the melt-spun $Ti_{40}Zr_{20}Hf_{20}$ (Ni, Pd or Pt)$_{20}$ and arc-melted $Ti_{40}Zr_{20}Hf_{20}Pt_{20}$ alloys are shown in Fig. 1. A single I phase was obtained in the melt-spun $Ti_{40}Zr_{20}Hf_{20}Ni_{20}$ alloy while amorphous and I phases were formed in the melt-spun $Ti_{40}Zr_{20}Hf_{20}Pd_{20}$ and $Ti_{40}Zr_{20}Hf_{20}Pt_{20}$ alloys. Indexing of I phase was carried out according to Ref. [20]. Here one should note that the (110000) peak position for $Ti_{40}Zr_{20}Hf_{20}Pd_{20}$ alloy does not correspond precisely to that of the I-phase.

The average size of the quasicrystalline particles in the melt-spun $Ti_{40}Zr_{20}Hf_{20}Ni_{20}$ alloy is 30 nm (Fig. 2(a)), which has been reported in one of our previous papers [19], while the average sizes of quasicrystalline particles in the melt-spun $Ti_{40}Zr_{20}Hf_{20}Pd_{20}$ and $Ti_{40}Zr_{20}Hf_{20}Pt_{20}$ alloys are 10 nm and 15 nm, respectively (Fig. 3(a) and Fig. 4(a)). The icosahedral particles have an equiaxed morphology.

Although the SAED patterns of the melt-spun $Ti_{40}Zr_{20}Hf_{20}Pd_{20}$ alloy (Fig. 3) indicate icosahedral symmetry, one can suggest these clusters are either distorted or belong to a high-order approximant phase.

A mixed structure consisting of I phase, big cubic face-centered cubic (fcc) cF96 Hf_2 Pt and body-centered cubic (bcc) cI2 β-(Ti, Zr, Hf, Pt) solid solution phases was observed in the $Ti_{40}Zr_{20}Hf_{20}Pt_{20}$ ingot (Fig. 1(d) and Fig. 5). The indexing of an even-parity sequence a,b,c,d and an odd-parity sequence A,B for the two-fold

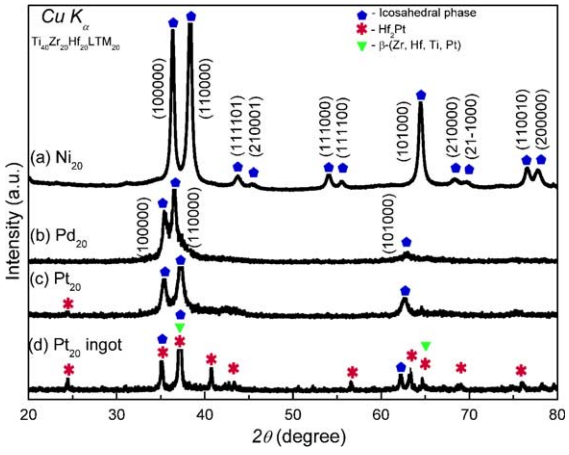

Fig. 1. XRD patterns of the melt-spun (a) $Ti_{40}Zr_{20}Hf_{20}Ni_{20}$, (b) $Ti_{40}Zr_{20}Hf_{20}pd_{20}$ and (c) $Ti_{40}Zr_{20}Hf_{20}Pt_{20}$ alloys and (d) the $Ti_{40}Zr_{20}Hf_{20}Pt_{20}$ ingot.

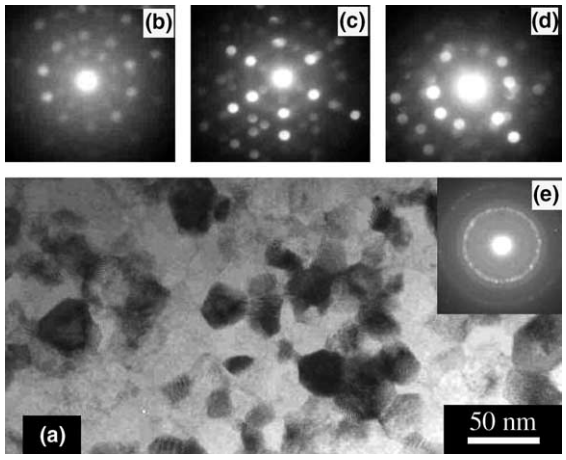

Fig. 2. TEM of the melt-spun $Ti_{40}Zr_{20}Hf_{20}Ni_{20}$ alloy: (a) bright-field image, (b), (c) and (d) nanobeam diffraction patterns of five-, three- and two-fold symmetries; and (e) selected-area electron diffraction pattern.

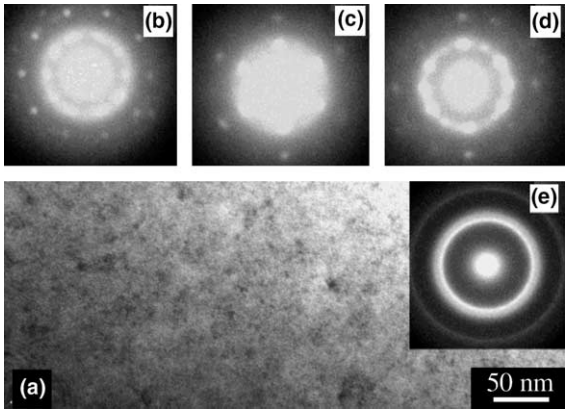

Fig. 3. TEM of the melt-spun $Ti_{40}Zr_{20}Hf_{20}Pd_{20}$ alloy: (a) bright-field image, (b), (c) and (d) nanobeam diffraction patterns of five-, three- and two-fold symmetries and (e) selected-area electron diffraction pattern.

pattern of the I phase (Fig. 5(b)) according to Ref. [21] is shown in Table 1. By using the diffraction peak of (332002) labeled as 6, the lattice parameter of I phase was calculated to be 0.5398 nm, which is slightly larger than the I phase formed in the melt-spun $Ti_{40}Zr_{20}Hf_{20}Pt_{20}$ alloy of a_q = 0.5346 nm.

A comparison of the structure of the melt-spun and the arc-melted $Ti_{40}Zr_{20}Hf_{20}Pt_{20}$ alloys was carried out. From the XRD pattern of the $Ti_{40}Zr_{20}Hf_{20}Pt_{20}$ ingot, the diffraction peaks of fcc Hf_2Pt phase partially coincide with the peaks of the I phase. From Fig. 1(d) Hf_2Pt phase has the largest volume fraction in the $Ti_{40}Zr_{20}Hf_{20}Pt_{20}$ ingot.

Fig. 6(b) and (c) shows that short-range distorted icosahedral clusters exist in the cF96 Hf_2Pt phase. Certainly the clusters do not have perfect icosahedral symmetry (Fig. 6(a)).

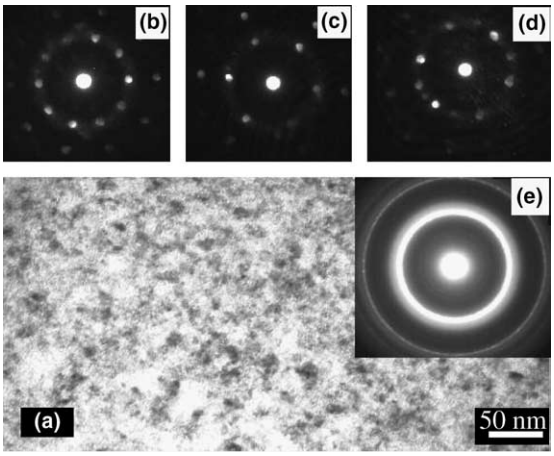

Fig. 4. TEM result of the melt-spun $Ti_{40}Zr_{20}Hf_{20}Pt_{20}$ alloy: (a) bright-field image, (b), (c) and (d) nanobeam diffraction patterns of five-, three- and two-fold symmetries; and (e) selected-area electron diffraction pattern.

One can suggest that formation of the I-phase upon solidification triggers nucleation and growth of the fcc cF96 Hf_2Pt+bcc cI2 β-(Ti, Zr, Hf, Pt) solid solution eutectic in the $Ti_{40}Zr_{20}Hf_{20}Pt_{20}$ ingot.

The results obtained provide one more piece of proof to support the suggestion that an icosahedral short-range order exists in the melt of $Ti_{40}Zr_{20}Hf_{20}Pt_{20}$ alloy just like in the Zr–Pt binary alloy [16–18]. During the rapid solidification (melt-spinning) the process of long-range diffusional rearrangement of atoms forming a stable crystalline phase has been suppressed. However, the lower cooling rate obtained for the ingot enables a long-range diffusion of atoms to form the equilibrium crystalline phases in addition to I phase.

The reason why the lattice parameter of I phase in the ingot is slightly larger than that in the melt-spun ribbon samples can also be explained based on the necessity of long-range rearrangement of atoms for precipitation and growth of the crystalline phases upon cooling. Thus, the chemical composition of the I-phase in the ingot is different from that in the melt-spun ribbon samples. In the ingot, the I-phase composition is much closer to equilibrium.

Table 1
Indexing of an even-parity sequence a,b,c,d and an odd-parity sequence A,B for the two-fold pattern of the I phase with the icosahedral quasicrystal lattice parameter $a_q = 0.5398$ nm

	Index	Label	Q experimental (nm^{-1})	Q calculated (nm^{-1})
B	100000	22	5.67	5.82
d	110000	21	9.87	9.90
c	111100	19	16.04	16.02
A	211111	16	24.67	24.65
b	221001	15	25.90	25.92
a	332002	6	41.94	41.94

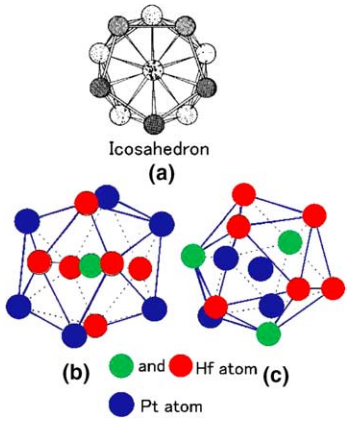

Fig. 6. (a) Icosahedral cluster (b) and (c) polyhedral clusters in cF96 Hf_2Pt phase.

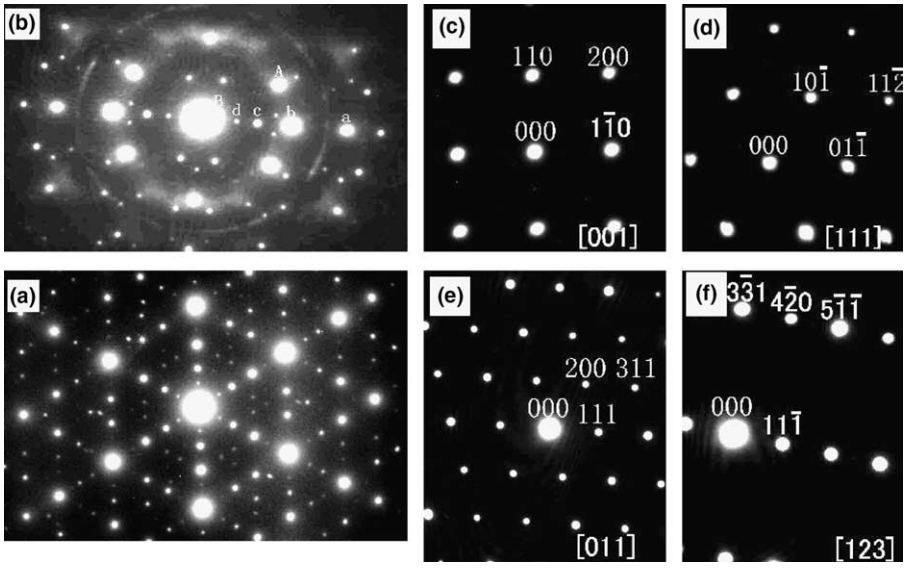

Fig. 5. Selected-area electron diffraction patterns from the phases observed in the $Ti_{40}Zr_{20}Hf_{20}Pt_{20}$ ingot: (a) three-fold and (b) two-fold symmetry of I phase (c) and (d) bcc β-(Ti, Zr, Hf, Pt) solid solution (e) and (f) fcc Hf_2Pt phase.

It is important to note that the icosahedral phase in Zr-based alloys is often formed in cooperation with cI2 β-Zr solid solution phase and these two phases have well defined orientation relationships [22]. Moreover, transformation from glassy+β-Zr to glassy+I structure was observed in $Zr_{65}Ni_{10}Al_{7.5}Cu_{7.5}Ti_5Nb_5$ alloy on heating by a single-stage transformation [23].

Although I phase-forming ability is greatest in the melt-spun $Ti_{40}Zr_{20}Hf_{20}Ni_{20}$ alloy, the addition of Pd and Pt can improve the glass-forming ability because of the larger heat of mixing with early transition metal elements [24–26].

4. Conclusions

Nanoscale I phase was found to form in the melt-spun $Ti_{40}Zr_{20}Hf_{20}LTM_{20}$ alloys. Ni is the most effective element for the formation of I phase while Pd and Pt slightly improve the glass forming ability of the Ti–Zr–Hf–LTM alloys. However, in Pd-bearing alloy it is presumed to be a distorted I-phase or a high-order approximant. I phase, cF96 fcc Hf_2Pt and β-(Ti, Zr, Hf, Pt) solid solution phases are formed in the arc-melted ingot of the $Ti_{40}Zr_{20}Hf_{20}Pt_{20}$ alloy.

References

[1] Shechtman D, Blech I, Gratias D, Cahn JW. Phys Rev Lett 1984;53:1951.
[2] Koster U, Eckert J, Loser W, Schultz L. Appl Phys Lett 1996;69:179.
[3] Xing LQ, Eckert J, Loser W, Schultz L. Appl Phys Lett 1998;73:2110.
[4] Inoue A, Zhang T, Chen MW, Sakurai T, Saida J, Matsushita M. J Mater Res 2000;15:2195.
[5] Louzguine DV, Ko MS, Inoue A. Appl Phys Lett 2000;76:3424.
[6] Li C, Saida J, Matsushita M, Inoue A. Appl Phys Lett 2000;77:528.
[7] Louzguine DV, Inoue A. Scripta Mater 2003;48:1325.
[8] Louzguine DV, Inoue A. J Alloys Compd 2003;361:153.
[9] Guo JQ, Tsai AP. Philos Mag Lett 2002;82:349.
[10] Guo JQ, Abe E, Tsai AP. Phys Rev B 2000;62:605.
[11] Kaneko Y, Maezawa R, Kaneko H, Ishimasa T. Philos Mag Lett 2002;82:483.
[12] Kelton KF, Kim WJ, Stroud RM. Appl Phys Lett 1997;70:3230.
[13] Kelton KF, Gibbons PC. MRS Bull 1997;22:69.
[14] Viano AM, Stroud RM, Gibbons PC, McDowell AF, Conradi MS, Kelton KF. Phys Rev B 1995;51:12026.
[15] Qiang JB, Wang YM, Wang DH, Kramer M, Thiel P, Dong C. J Non-Cryst Solids 2004;334 & 335:223.
[16] Saida J, Matsushita M. Appl Phys Lett 2000;77:73.
[17] Saida J, Matsushita M, Inoue A. J Non-Cryst Solids 2002;342:18.
[18] Kitada M, Imafuku M, Saida J, Inoue A. J Non-Cryst Solids 2002;312–314:594.
[19] Chen N, Louzguine DV, Ranganathan S, Inoue A. Acta Mater 2005;53:759.
[20] Bancel PA, Heiney PA, Stephens PW, Goldman AI, Horn PM. Phys Rev Lett 1985;54:2422.
[21] Elaser V. Phys Rev B 1985;32:4892.
[22] Yang XY, Kramer MJ, Rozhkova EA, Sordelet DJ. Scripta Mater 2003;49:885.
[23] Louzguine DV, Ouyang LJ, Kimura HM, Inoue A. Scripta Mater 2004;50:973.
[24] Inoue A. Mater Trans 1995;36:866.
[25] Inoue A. Acta Mater 2000;48:277.
[26] Inoue A, Zhang T, Saida J, Matsushita M. Mater Trans 2000;41:1511.